Aust. J. Phys., 1996, **49**, 383–401

Spin Effects in the (e, 2e) Cross Section of Xenon*

B. Granitza,[A] *X. Guo, J. M. Hurn, J. Lower, S. Mazevet, I. E. McCarthy,*[B] *Y. Shen*[C] *and E. Weigold*

Research School of Physical Sciences and Engineering,
Australian National University,
Canberra ACT 0200, Australia.
[A] Present address: Laserlaboratorium Göttingen e.V.,
Hans-Adolf-Krebs-Weg 1, D-37077 Göttingen, Germany.
[B] ESM Centre, Flinders University of South Australia,
GPO Box 2100, Adelaide, SA 5001, Australia.
[C] Present address: Faculty of Science and Technology,
Griffith University, Nathan, Qld 4111, Australia.

Abstract

In a series of experiments investigating the spin-dependent aspects of electron impact induced ionisation of atoms with a spin-resolved incident electron beam we have measured spin-resolved (e, 2e) cross sections for xenon. By experimentally resolving the fine structure levels of the ground state residual ion the existence of an effect analogous to the fine structure effect in excitation has been established, whereby strong and opposite polarisation effects are observed in the ionisation of a spinless closed shell target leading to a fine structure doublet.

1. Introduction

Over recent years there has been steady improvement in our understanding of electron impact ionisation processes. Nevertheless, interesting new aspects continue to emerge as attention now focuses on finer details of the problem. One of the driving forces has been the improved state selectivity of recent experiments which now permit the measurement of many partial cross sections for the first time. In general, the most detailed information concerning electron impact ionisation is derived from (e, 2e) experiments, in which the energy and momentum channels of all reaction participants are determined (McCarthy and Weigold 1976, 1991).

Until recently, all (e, 2e) experiments were performed with unpolarised primary electron beams and unpolarised targets. Although such experiments provide detailed information on the role of the Coulomb interaction during the collision, the cross section is not explicitly dependent on the weaker spin-dependent components of the scattering potential as the experiment does not resolve the

* Refereed paper based on a contribution to the Advanced Workshop on Atomic and Molecular Physics, held at the Australian National University, Canberra, in February 1995.

0004-9506/96/020383$10.00

individual spin-dependent reaction channels. Mathematically, the spin-unresolved (e, 2e) cross section can be expressed as

$$\frac{\mathrm{d}^5\sigma}{\mathrm{d}\Omega_\mathrm{s}\,\mathrm{d}\Omega_\mathrm{f}\,\mathrm{d}E_\mathrm{f}} =$$

$$(2\pi)^4\,\frac{p_\mathrm{s}\,p_\mathrm{f}}{p_0}\,\frac{1}{2(2J_\mathrm{A}+1)}\sum_{v_0 v_\mathrm{s} v_\mathrm{f} M_\mathrm{A} M_\mathrm{i}} |\langle \boldsymbol{p}_\mathrm{s}\, v_\mathrm{s}\, \boldsymbol{p}_\mathrm{f}\, v_\mathrm{f}\, J_\mathrm{i}\, M_\mathrm{i}|T|J_\mathrm{A}\, M_\mathrm{A}\, \boldsymbol{p}_0\, v_0\rangle|^2 . \qquad (1)$$

The subscripts 0, s and f refer respectively to the incident and the final state continuum electrons. The symbols Ω_f and Ω_s refer to the solid angles of emission for both final state electrons and E_f to the energy of one of them; A denotes the atomic target and i the residual ion; J and M represent the quantum numbers for total angular momentum and its projection for the initial and final atomic and ionic states; $\boldsymbol{p}$ and v are used to denote respectively the linear momenta and the spin projections of the continuum electrons; and T is the transition operator for the reaction. The expansion is fully antisymmetrised.

A first step to gaining more precise information on the spin interactions is to use a polarised electron beam in conjunction with a polarised or spin-zero atomic target. In this case the summations in equation (1) over the spin direction of the incident electron and the magnetic states of the target atom disappear, significantly reducing the number of spin-dependent reaction channels over which the experiment is averaging. Such experiments are still in their infancy (Baum *et al.* 1992; Prinz *et al.* 1995; Granitza *et al.* 1993; Simon *et al.* 1993). Elimination of the summation over v_s and v_f (for M_i non-zero) requires the employment of spin-sensitive detectors for the two final state continuum electrons as well as determination of the angular momentum projection of the residual ion. To date however, no experiment has approached this level of complexity.

Not only the level of state selectivity, but also the choice of (e, 2e) reaction kinematics is critical in determining the sensitivity of the measured cross section to spin-dependent effects. Careful selection of the kinematics enables details of either the ionisation mechanism or of target structure to be highlighted. An illustration of the power of the (e, 2e) technique for structure determination is given in the paper by Brunger (1996; this issue p. 347). By performing experiments at high energies under so-called non-coplanar geometry, equation (1) simplifies to a form whereby the measured (e, 2e) cross section gives direct information on the spectral momentum density of target electrons. To highlight details of the ionisation mechanism, on the other hand, lower energies and the so-called coplanar geometry are usually preferred in which the momenta of all electrons involved in the collision are confined to a common plane (Ehrhardt 1986).

The present work involves (e, 2e) scattering of polarised electrons from a spin-zero xenon target in which the angular momentum state J_i of the residual ion is resolved. Coplanar asymmetric geometry has been employed, in which the energies and scattering angles of the two final state electrons are unequal (Fig. 1).

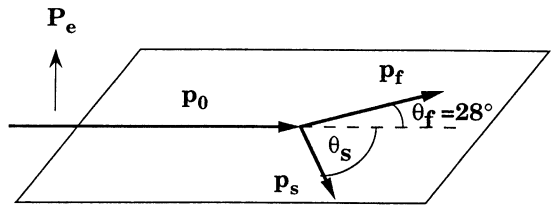

Fig. 1. Kinematics for the present coplanar asymmetric (e, 2e) experiments on ground state xenon, where p_0, p_f and p_s correspond to the incident, fast and slow electron momenta respectively. The incident beam energy is fixed at 147 eV. Fast scattered electrons of average energy 100 eV are detected at an angle θ_f of 28° to the left of the of the primary beam, looking along the primary beam direction. Here θ_s is the scattering angle for the slow scattered electrons of mean energy 35 eV which is scanned in the experiment, while P_c represents the incident beam polarisation vector directed perpendicular to the reaction plane.

2. Analogue to the 'Fine Structure Effect' in Ionisation

In the process of electron impact ionisation, there are a number of spin-dependent processes to consider. Firstly there is spin–orbit interaction of the continuum electrons in the atomic and ionic fields, which produces spin flips for the continuum electrons under conditions where conservation of total spin for the electron–atom system no longer holds. Even for ionisation at low incident energies, significant contributions to the ionisation cross section from these spin–orbit interactions could still be expected for the case of heavy targets, since this is the case for elastic scattering (Kessler 1985). Spin-orbit interactions in the target and residual ion, on the other hand, lead to modification of their respective wave functions and to fine structure splitting. Finally, there is the process of exchange to consider, occurring between incident and target electrons and between the two final state continuum electrons. All of these processes together determine the final form of the ionisation cross section.

It has been suggested by Hanne (1991) that in the ionisation of unpolarised closed shell atoms by polarised electrons, special spin effects may be observed in the (e, 2e) ionisation cross section if the fine structure levels of the residual ion state are resolved in the experiment. The postulated effect would still be present even in the limit of negligible spin–orbit interaction of the continuum electrons and is analogous to the so called 'fine structure effect' in excitation (Kessler 1992; Dümmler *et al.* 1995), where a spin-asymmetry results from an interplay between the processes of collisionally induced orientation of the target atom and exchange between incident and target electrons. In the case of ionisation, spin asymmetries would result from collisionally induced orientation of the residual ion core and from exchange between the incident and core electrons and between the final state continuum electrons.

To illustrate how such an effect might arise, we consider here the ionisation of xenon by polarised electrons leading to the $5p^5\ P_{1/2}$ residual ion state. For the purposes of illustration, the approximation is made that the final state can be described as an *LS* coupled system and that the spin–orbit interaction of the continuum electrons is negligible. Under such conditions, spin will be conserved in the reaction. The following analysis is performed in the natural frame with

only the possibility of exchange between the two final state continuum electrons considered, amplitudes describing the process of capture not being included in the present model. In Table 1 the arrows ↑ and ↓ are used to denote the spin projections (positive or negative) for the continuum electrons and for the residual xenon ion along the quantisation axis perpendicular to the reaction plane. The symbols $f_{\pm 1}$ and $g_{\pm 1}$ denote the ionisation amplitudes for direct and exchange processes respectively corresponding to cases where the residual ion is left in either the $m_l = +1$ or $m_l = -1$ orbital angular momentum state. The three possible reactions leading to the $^2P_{1/2}$ state are listed in Table 1.

Table 1. The three possible reactions leading to the $^2P_{1/2}$ state with their corresponding partial cross sections

Initial state	Final state: Ion			Electron	Electron	Cross section
	$Xe^+ {}^2P_{1/2}$	m_s	m_l	$(E_f, \boldsymbol{p}_f)$	$(E_s, \boldsymbol{p}_s)$	
$e(\uparrow)+Xe(^1S_0)$	$Xe^+(\downarrow)$	$-\frac{1}{2}$	$+1$	$e(\uparrow)$	$e(\uparrow)$	$\lvert f_{+1} - g_{+1}\rvert^2$
	$Xe^+(\uparrow)$	$+\frac{1}{2}$	-1	$e(\uparrow)$	$e(\downarrow)$	$\lvert f_{-1}\rvert^2$
	$Xe(\uparrow)$	$+\frac{1}{2}$	-1	$e(\downarrow)$	$e(\uparrow)$	$\lvert g_{-1}\rvert^2$

In the first reaction, the spin orientation of the ion is negative and hence the orientation of the orbital angular momentum vector must be positive. Due to the indistinguishability of the two final state continuum electrons it is not possible to establish whether the reaction has occurred through a direct or an exchange process. That is, whether the incident electron has been scattered to the left, loosing energy $E_0 - E_s - \epsilon_{1/2}$ and momentum $\boldsymbol{p}_0 - \boldsymbol{p}_s - \boldsymbol{q}$ in the process, or to the right with energy and momentum losses of $E_0 - E_f - \epsilon_{1/2}$ and $\boldsymbol{p}_0 - \boldsymbol{p}_f - \boldsymbol{q}$ respectively. Here $\epsilon_{1/2}$ represents the xenon ionisation energy for the reaction leading to a $5p^5\ {}^2P_{1/2}$ final ion state and $\boldsymbol{q}$ the recoil momentum of the residual ion after the collision. Thus the amplitudes for both direct and exchange processes must be summed coherently in calculating the ionisation cross section leading to the $m_l = +1$ final ion state.

The second and third reactions describe ionisation occurring through direct and exchange processes respectively where the residual ion is left in a state of positive spin (negative orbital angular momentum) orientation. These two reactions are distinguishable from one another as the two final state continuum electrons have opposite spin and because the spin projection of the continuum electrons is preserved in the scattering process, under our assumption that spin–orbit interaction of the continuum electrons is negligible. The cross section leading to the $m_l = -1$ final ion state is thus described by the incoherent sum of amplitudes describing ionisation by direct and exchange processes.

The differential ionisation cross section $\sigma^{\uparrow}_{1/2}$ for ionisation leading to the $J = \frac{1}{2}$ final ion state by incident spin-up electrons can thus be written as a sum of the following three terms:

$$\sigma^{\uparrow}_{1/2} = K\tfrac{2}{3}[|f_{+1} - g_{+1}|^2 + |f_{-1}|^2 + |g_{-1}|^2]\,. \tag{2}$$

Here K is a constant dependent only on the kinematics. Similarly for ionisation by spin-down electrons, one obtains the relation

$$\sigma_{1/2}^{\downarrow} = K\tfrac{2}{3}[|f_{-1} - g_{-1}|^2 + |f_{+1}|^2 + |g_{+1}|^2]\,. \tag{3}$$

For ionisation to a final ion state of non-zero orbital angular momentum, it has been well established (Anderson *et al.* 1988) that the Coulomb force alone can orient the residual ion in the collision process. In this case, $f_{+1} \neq f_{-1}$ and from equations (2) and (3) above, implies that the cross section $\sigma_{1/2}^{\uparrow}$ for ionisation by spin-up electrons is in general different from that for ionisation by spin-down electrons, $\sigma_{1/2}^{\downarrow}$. A non-zero spin asymmetry $A_{1/2}$ for the $J = \frac{1}{2}$ transition thus results, where $A_{1/2}$ is defined by the relation

$$A_{1/2} = \frac{\sigma_{1/2}^{\uparrow} - \sigma_{1/2}^{\downarrow}}{\sigma_{1/2}^{\uparrow} + \sigma_{1/2}^{\downarrow}}\,. \tag{4}$$

Note that in the limit of either the direct amplitude f or the exchange amplitude g going to zero, the asymmetry disappears, the asymmetry itself resulting from an interference between amplitudes describing ionisation through direct and exchange processes when the two final state electrons have the same spin projection.

In the paper of Jones *et al.* (1994), similar expressions were derived for ionisation leading to the $5p^5\ {}^2P_{3/2}$ ion state. Their analysis was performed under the LS coupling scheme with an independent particle Hartree–Fock description of both initial target and final ionic states. Again both the processes of capture and spin–orbit interaction of the continuum electrons were neglected in their treatment. Making the assumption that the ionisation amplitudes for direct scattering $f_{\pm 1}$ and exchange scattering $g_{\pm 1}$ are independent of the final ion state $J_f = \frac{1}{2}$ or $J_f = \frac{3}{2}$, their analysis predicts that no spin asymmetry will be observed if the fine structure levels of the final ion state are not resolved, i.e.

$$\sigma_{1/2}^{\uparrow} + \sigma_{3/2}^{\uparrow} = \sigma_{1/2}^{\downarrow} + \sigma_{3/2}^{\downarrow}\,. \tag{5}$$

This result is in complete analogy to a pure fine structure effect for excitation where no spin asymmetry exists when the fine structure levels of the excited state are unresolved (Hanne 1983). Their analysis showed the asymmetries for the ${}^2P_{1/2}$ and ${}^2P_{3/2}$ final state transitions to be related by the expression

$$A_{1/2} = -2A_{3/2}\,, \tag{6}$$

and the unpolarised (spin-averaged) cross sections $\sigma_{1/2}$ and $\sigma_{3/2}$ by the equation

$$\sigma_{3/2} = 2\sigma_{1/2}\,, \tag{7}$$

where

$$\sigma_{1/2} = (\sigma_{1/2}^{\uparrow} + \sigma_{1/2}^{\downarrow})/2 \quad \text{and} \quad \sigma_{3/2} = (\sigma_{3/2}^{\uparrow} + \sigma_{3/2}^{\downarrow})/2\,. \tag{8}$$

Part of the aim of the present work was to test the validity of these hypotheses.

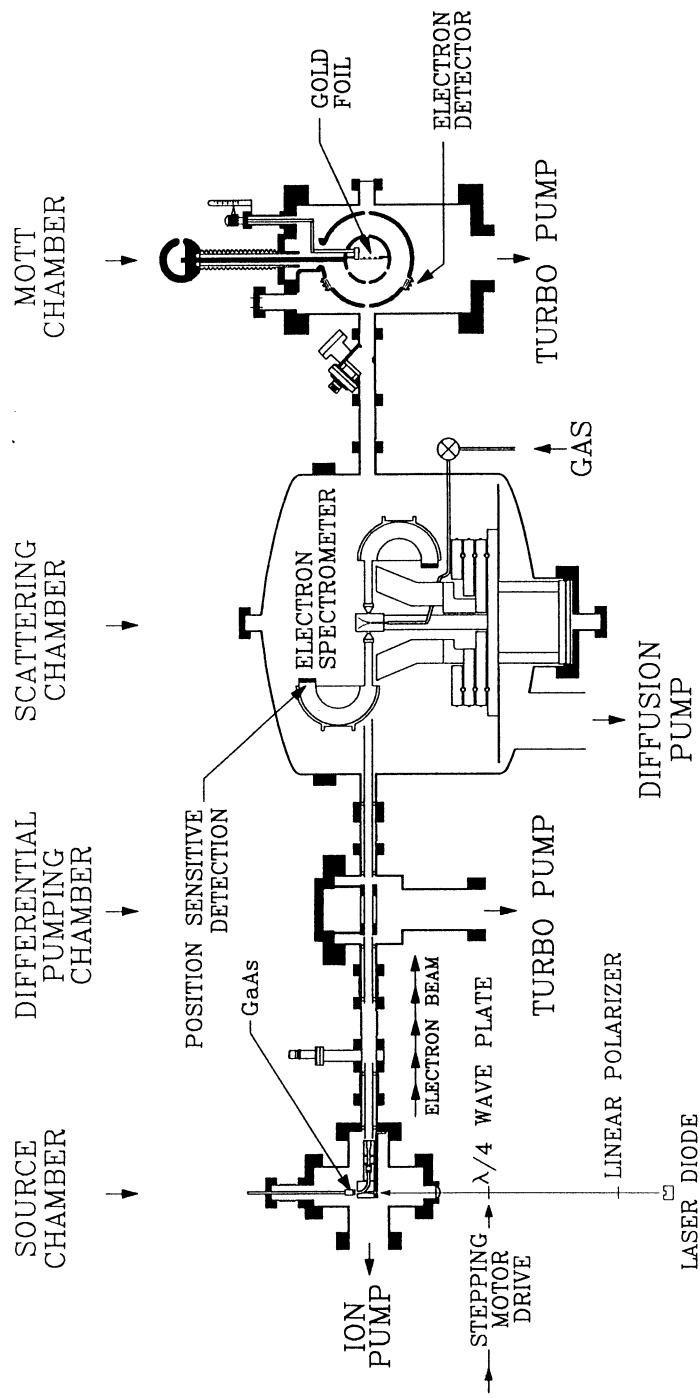

Fig. 2. Experimental apparatus for measuring spin-resolved ionisation cross sections for gaseous targets showing the polarised electron source, differential pumping chamber, collision chamber and Mott detector (see text for details).

3. Apparatus

Fig. 2 shows schematically the experimental apparatus used for the present measurements. The coincidence spectrometer consists of four vacuum chambers, referred to respectively as the source, differential, scattering and Mott chambers. All reside within a series of large Helmholtz coils whose function is to compensate for external magnetic fields. Apart from causing unwanted deviations in the electron trajectories, stray magnetic fields produce rotations in the polarisation direction of polarised electron beams.

The source chamber houses the GaAs photocathode, from which polarised electrons are extracted after its irradiation by circularly polarised light of 810 nm wavelength. This circularly polarised light is provided by passing the output of a GaAlAs laser operated in CW mode through a quarter wave plate. The photocathode is prepared from a GaAs crystal substrate, first chemically cleaned outside the chamber and then cleaned in situ by heating to 960 K. Its [100] surface is activated by coating with successive layers of Cs and O_2 to produce a surface of negative electron affinity (Pierce *et al.* 1980). This chamber, pumped by a 30 l/s ion pump and a titanium sublimation pump, is maintained at pressures better than 2×10^{-10} Torr to minimise the contamination rate to the crystal surface from background gas, and thereby minimise the frequency of required cleaning and activation cycles. The initially longitudinally polarised electron beam is converted to one of transverse polarisation after deflection through 90° by an electrostatic field, the field acting on the beam trajectory but not on its polarisation direction. Inversion of the polarisation direction of the incident beam is effected by reversing the helicity of the laser light incident upon the GaAs photocathode. This is achieved through rotation of a quarter wave plate located between the laser diode and the photocathode.

After extraction from the photocathode, the beam passes through a series of electrostatic lenses in which it is focussed and accelerated to 1000 eV. With this energy it passes through the differential chamber, pumped by a 180 l/s turbo molecular pump, to the main scattering chamber where it is decelerated to the impact energy required for the (e, 2e) ionisation experiment. Transporting the beam from the source to the scattering chamber at a higher energy has two advantages. Firstly, it renders the beam less sensitive to the effects of deflection, defocussing and to rotation of its spin-polarisation direction caused by stray magnetic fields (Kessler 1985). Secondly, the narrower beam profile obtainable at higher beam energies enables small apertures to be introduced along the beam path, allowing a large pressure gradient to be maintained between the source and scattering chambers. Indeed, under operating conditions the inclusion of these apertures and the presence of the differential chamber, whose role is to act as a differential pumping stage, enables a pressure difference of four orders of magnitude to be established between the source and scattering chambers during an experiment.

The (e, 2e) events are measured in the scattering chamber by two rotatable 180° hemispherical electrostatic analysers. They are both confined to the reaction plane, defined by the momentum vectors of the incident and measured scattered electrons and containing the incident electron beam. The input optics for each analyser consists of a five element cylindrical lens stack allowing semi-independent

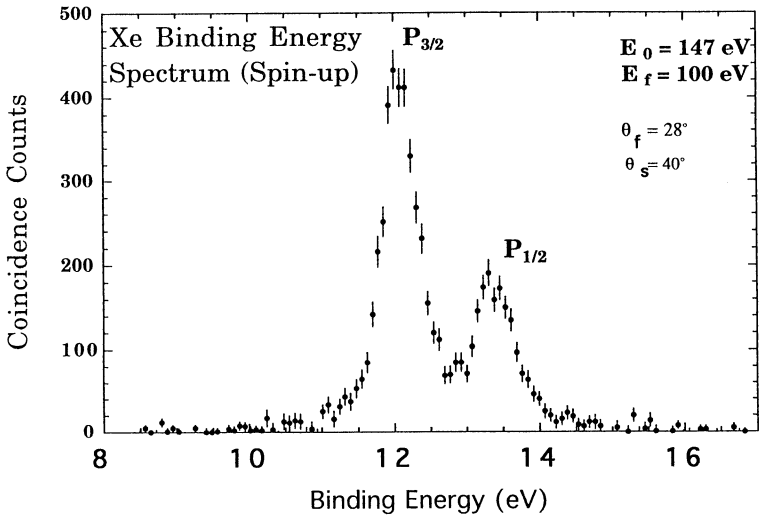

Fig. 3. Xenon binding energy spectrum showing transitions to the Xe^+ $5p^5$ $^2P_{1/2}$ and $^2P_{3/2}$ ion states resulting from ionisation by spin-up incident electrons. Slow scattered electrons of mean energy 35 eV were recorded at a scattering angle θ_s of 40°. All other kinematical variables are as defined in Fig. 1.

recorded for an identical accumulation time. From the two spectra, the corrected measured (e, 2e) count rates $N_J^{\uparrow}$ and $N_J^{\downarrow}$ for incident spin-up and spin-down electrons respectively are extracted for the individual $^2P_{1/2}$ and $^2P_{3/2}$ transitions. The partial overlap of the two peaks is taken into account by fitting the data with the instrument response function. Of primary interest is the determination of the spin-resolved relative (e, 2e) cross sections $\sigma_J^{\uparrow}$ and $\sigma_J^{\downarrow}$ respectively for spin-up and spin-down incident electrons. These relative cross sections are determined from the count rates $N_J^{\uparrow}$ and $N_J^{\downarrow}$ by subtracting the contribution of the unpolarised component of the incident electron beam through the expressions

$$\sigma_J^{\uparrow} = \frac{1}{2P_e}[(1+P_e)N_J^{\uparrow} - (1-P_e)N_J^{\downarrow}], \tag{10}$$

$$\sigma_J^{\downarrow} = \frac{1}{2P_e}[(1+P_e)N_J^{\downarrow} - (1-P_e)N_J^{\uparrow}]. \tag{11}$$

To highlight different aspects of the scattering problem, it is useful to present the results in a number of forms. Unpolarised (spin-averaged) relative cross sections for ionisation to the $J = \frac{1}{2}$ and $J = \frac{3}{2}$ ion states have been determined from equation (8). Spin asymmetries, given by the expression

$$A_J = \frac{\sigma_J^{\uparrow} - \sigma_J^{\downarrow}}{\sigma_J^{\uparrow} - \sigma_J^{\downarrow}}, \tag{12}$$

are also presented, as are spin resolved and unresolved branching ratios, $R^{\uparrow}, R^{\downarrow}$

and R respectively, derived from the expressions

$$R^{\uparrow} = \sigma^{\uparrow}_{3/2}/\sigma^{\uparrow}_{1/2}, \qquad R^{\downarrow} = \sigma^{\downarrow}_{3/2}/\sigma^{\uparrow}_{1/2},$$

$$R = \sigma_{3/2}/\sigma_{1/2}. \tag{13}$$

The residual asymmetry A_{5p} for the transition leading to the unresolved Xe^+ $5p^5$ ion state is also given, calculated from the summed $^2P_{1/2}$ and $^2P_{3/2}$ cross sections in the following manner:

$$A_{5p} = \frac{(\sigma^{\uparrow}_{1/2} + \sigma^{\uparrow}_{3/2}) - (\sigma^{\downarrow}_{1/2} + \sigma^{\downarrow}_{3/2})}{(\sigma^{\uparrow}_{1/2} + \sigma^{\uparrow}_{3/2}) + (\sigma^{\downarrow}_{1/2} + \sigma^{\downarrow}_{3/2})}. \tag{14}$$

In the non-relativistic limit this quantity should be zero (cf. equation 6).

5. Discussion

Figs 4 to 13 show the experimental results compared with calculations performed within a distorted wave Born approximation (DWBA) formalism. The experimental branching ratios and asymmetry data presented by us in an earlier publication (Guo *et al.* 1995) appear here in a slightly revised form due to subsequent improvements made to our data extraction and analysis techniques. For the calculations of Jones *et al.* (1994), the asymmetry is expressed within the *LS* coupling scheme and describes essentially a pure fine structure effect

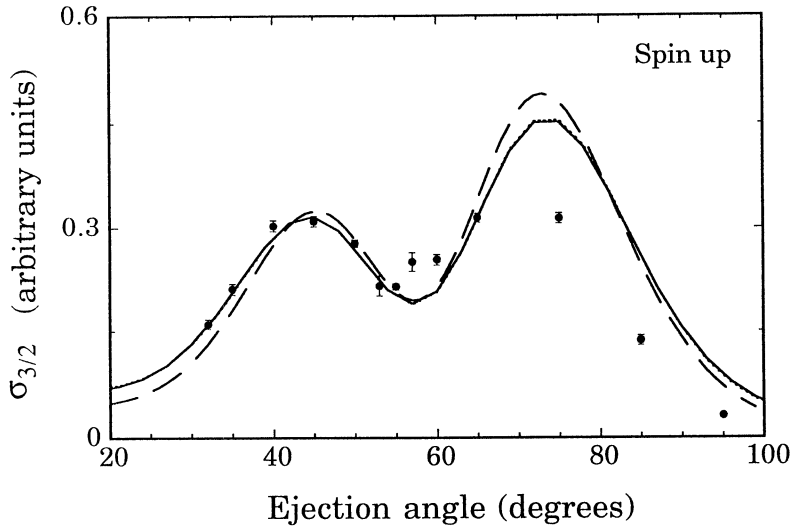

Fig. 4. Experimental and theoretical cross sections for the electron impact ionisation of the ground state Xe atom by spin-up incident electrons leading to the Xe^+ $5p^5$ $^2P_{3/2}$ ion state. Kinematics are as described in Fig. 1. The experimental results are compared with the following DWBA calculations (see text for details): Our calculations, non-relativistic with Hartree–Fock target wave functions (dotted curve) and semi-relativistic with Dirac–Fock target wave functions (solid curve); the calculation of Jones *et al.* (1994) using Dirac–Fock target wave functions (dashed curve).

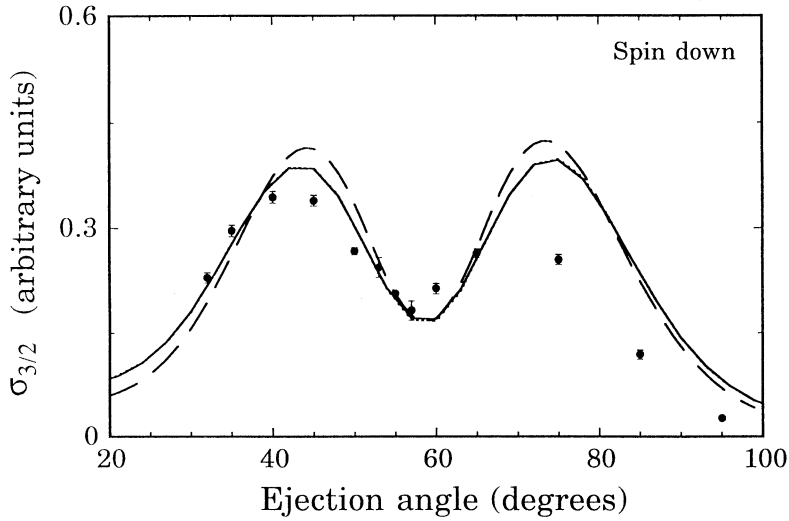

Fig. 5. As for Fig. 4, but for spin-down incident electrons. Comparison with Fig. 4 shows the strength of the transition leading to the Xe^+ $5p^5$ $^2P_{3/2}$ ion state depends strongly on the sign of the spin projection of the incident electrons along the quantisation axis perpendicular to the reaction plane.

with only a partial account being taken of the spin–orbit interaction of the continuum electrons through use of a Dirac–Fock wave-function for the target. In our theoretical approach, two calculations have been performed. The first is a non-relativistic DWBA calculation using Hartree–Fock wave-functions. The second is a semi-relativistic DWBA calculation employing Dirac–Fock wave-functions. For the latter case the distorted waves are calculated in the static exchange potential of the target or ion, as appropriate, with the addition of the Thomas spin–orbit term. The asymmetry parameter is expressed using the density matrix formalism to take into account both the contribution of the fine structure effect and the spin–orbit interactions for the continuum electrons.

Figs 4–7 show the results for the spin-resolved angular correlations for the $^2P_{1/2}$ and $^2P_{3/2}$ transitions derived using equations (10) and (11). Because the measured cross sections are relative and not absolute, the theories have all been normalised to the experimentally determined cross section for the $^2P_{3/2}$ transition at an ejection angle of 40° for the slow electron, after first averaging both theory and experiment over the spin direction of the incident electron. Fig. 4 shows the angular correlation for the $^2P_{3/2}$ transition for spin-up incident electrons compared with our non- and semi-relativistic DWBA calculations and the DWBA calculations of Jones *et al.* (1994). The cross section is dominated by two lobes, located at around 45° and 70° and separated by a minimum at around 55°. Such double-lobe angular behaviour is to be expected for the ionisation of a p electron in the binary region under Bethe-Ridge kinematics. In general the DWBA calculations are similar to the measurements, although they are unable to accurately predict the relative strengths and angular separations of the forward and backward lobes. Comparison of our theoretical results using Dirac–Fock wave functions with those of Jones *et al.* (1994) shows both results to be very

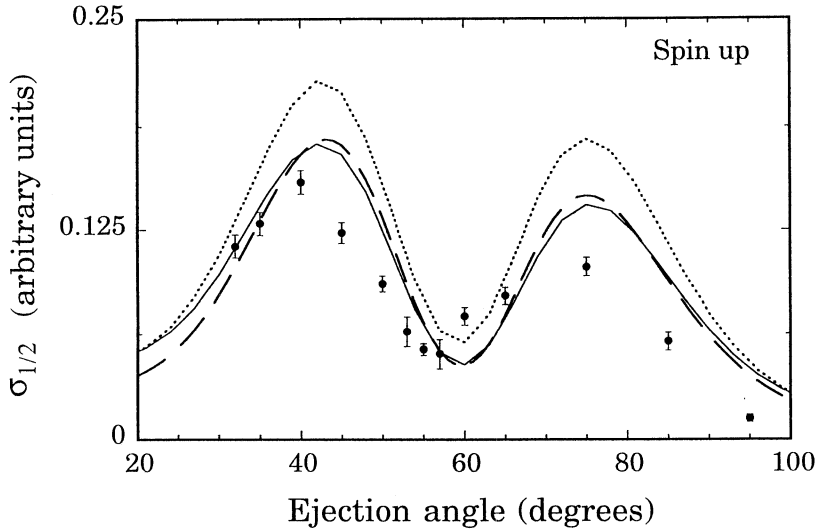

Fig. 6. Experimental and theoretical cross sections for the electron impact ionisation of the ground state Xe atom by polarised spin-up incident electrons leading to the Xe^+ $5p^5$ $^2P_{1/2}$ ion state. Reaction kinematics and theories are as described above.

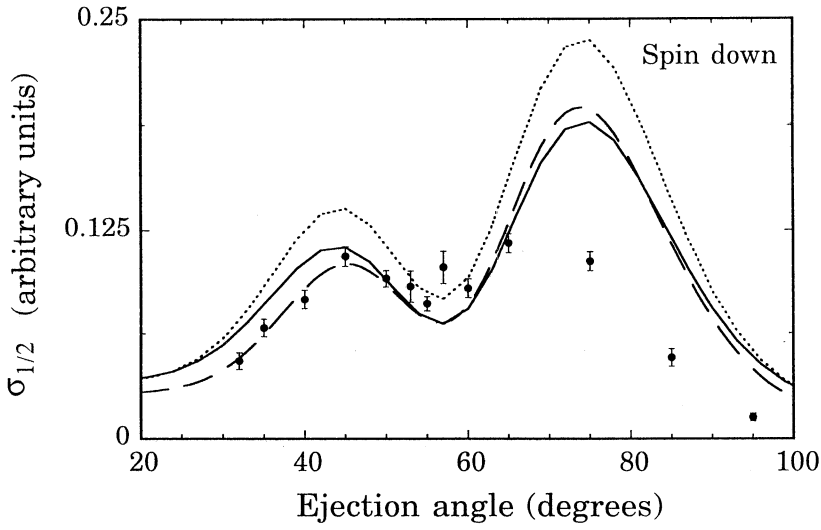

Fig. 7. As for Fig. 6, but for polarised spin-down incident electrons.

similar to one another, whilst the results from our non- and semi-relativistic DWBA calculations are virtually indistinguishable in shape from one another. Fig. 5 shows the angular correlation for the same transition but now for spin-down incident electrons. In contrast to Fig. 4, the experimental results show that the forward lobe around 45° is now noticeably larger in magnitude than the backward lobe, whereas for spin-up incident electrons it appeared to be of slightly smaller relative magnitude. The spin-dependent trend is confirmed by all of the

calculations, although again they are unable to accurately predict the relative strengths of and the angular separation between the forward and backward lobes.

In Figs 6 and 7 the angular correlations for the $^2P_{1/2}$ transition are presented for spin-up and spin-down incident electrons respectively and compared with calculations of the same theories. As predicted by equation (7), the cross sections are smaller for this transition. In contrast to the results for the $^2P_{3/2}$ transition, the 45° lobe is now the stronger of the two lobes for spin-up incident electrons and the weaker for spin-down electrons. A large discrepancy is now evident between the results of the calculation using Hartree–Fock wave functions and those using Dirac–Fock target wavefunctions. Only the calculations using a relativistic description of the target atom are able to accurately predict the relative strengths of the $^2P_{3/2}$ and $^2P_{1/2}$ transitions.

The asymmetries for the $^2P_{3/2}$ and $^2P_{1/2}$ transitions are presented in Figs 8 and 9 respectively. The experimental results substantiate the existence of a strong up–down asymmetry in the ionisation of the closed shell xenon target when the fine structure levels of the final ion state are resolved. The measured spin asymmetries for the $^2P_{3/2}$ and $^2P_{1/2}$ transitions are both large in magnitude and strongly dependent on the ejection angle of the slow electron. At any given ejection angle, the measured asymmetry values for the $^2P_{1/2}$ transition are approximately twice the magnitude but of opposite sign to those for the $^2P_{3/2}$ transition, in concordance with the prediction of equation (6) for the limiting case of negligible spin–orbit interaction and in the absence of the process of capture. The experimental results are again compared to the DWBA calculation by us and the results of Jones *et al.* (1994). In all cases, the agreement between calculations and experiment is quite good, although the existence of a small angular shift between all calculations and experiment is evident. In particular, the agreement between our non-relativistic and semi-relativistic calculations illustrates the insensitivity of the asymmetry calculation to the description of the target and the residual ion and suggests that the contributions to the measured asymmetries from the spin–orbit interaction of the continuum electrons in the atomic and ionic fields are small under the present kinematics.

It is interesting to note that the ejection angle for which theory predicts both asymmetries to change sign corresponds exactly to the condition where the residual ion recoil momentum is zero. This corresponds to the high symmetry kinematical condition in which the summed momentum of the two final state continuum electrons is parallel to and equals the momentum of the incident electron. For a given combination of energy values for the incident and two final state continuum electrons, this condition is satisfied only for a single unique pair of scattering angles for the continuum electron pair.

The spin-resolved branching ratios $\sigma^{\uparrow}_{3/2}/\sigma^{\uparrow}_{1/2}$ and $\sigma^{\downarrow}_{3/2}/\sigma^{\downarrow}_{1/2}$ are presented in Figs 10 and 11. Because the asymmetries for the $^2P_{1/2}$ and $^2P_{3/2}$ transitions are of opposite sign, the spin dependence of the ratios is large. Consistent with Figs 8 and 9, both branching ratios are equal at 48° where the asymmetries for the $^2P_{1/2}$ and $^2P_{3/2}$ transitions are zero. Agreement between calculations using relativistic descriptions of the target wave function and experiment is again quite good, whilst agreement between the non-relativistic calculation and experiment is much poorer, with this theory predicting significantly lower values than experiment over most of the angular range. Fig. 12 shows the spin-averaged branching ratio $\sigma_{3/2}/\sigma_{1/2}$

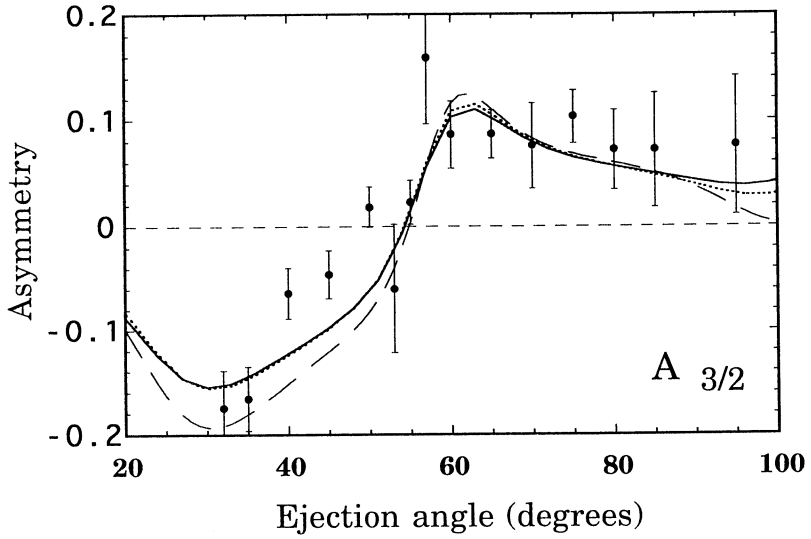

Fig. 8. Spin up–down asymmetries for the electron impact ionisation of a ground state Xe target leading to the Xe^+ $5p^5$ $^2P_{3/2}$ ion state. Strong polarisation effects are observed when the fine structure levels of the residual ion state are resolved. Comparison between our two calculations, using Hartree–Fock and Dirac–Fock wave functions respectively, shows the calculation of the asymmetry parameter to be insensitive to the description of the target wave function. Reaction kinematics and theories are as described above.

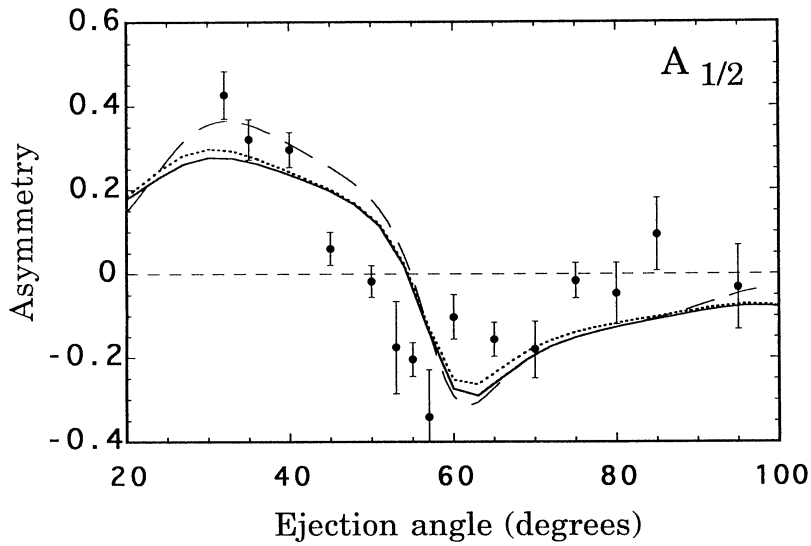

Fig. 9. Spin up–down asymmetries for the electron impact ionisation of a ground state Xe target leading to the Xe^+ $5p^5$ $^2P_{1/2}$ ion state. In accordance with the predictions for a 'pure' fine structure effect, the asymmetries $A_{1/2}$ for the $^2P_{1/2}$ transition (Fig. 8) and $A_{3/2}$ for the $^2P_{3/2}$ transition (present figure) are related approximately by the expression $A_{1/2} = -2A_{3/2}$.

derived using equation (8). Immediately obvious are the strong deviations from the ratio of 2 predicted by equation (7) in the limit of vanishingly small spin–orbit effects and in the absence of capture for the $^2P_{1/2}$ and $^2P_{3/2}$ transitions. We note that the reason our non-relativistic DWBA calculation using Hartree–Fock

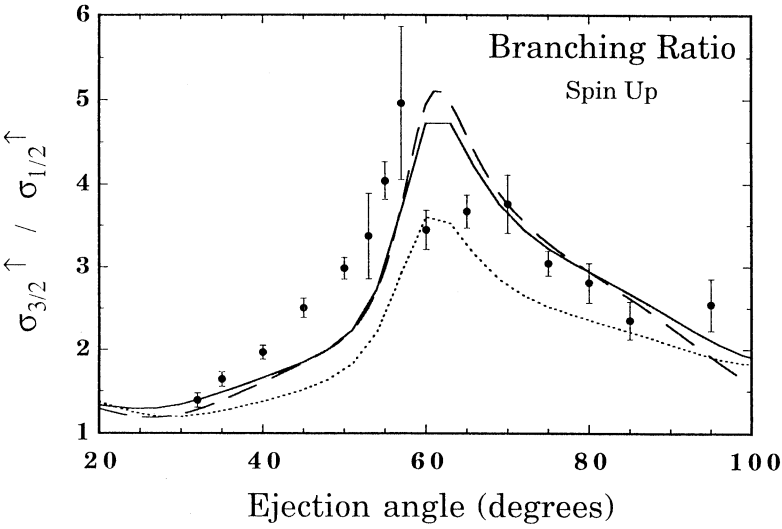

Fig. 10. Spin-resolved branching ratio $\sigma^{\uparrow}_{3/2}/\sigma^{\uparrow}_{1/2}$ for the electron impact ionisation of a ground state Xe target by spin-up incident electrons leading to the Xe^+ $5p^5$ $^2P_{1/2}$ and $^2P_{3/2}$ ion states. Reaction kinematics and theories are as described above.

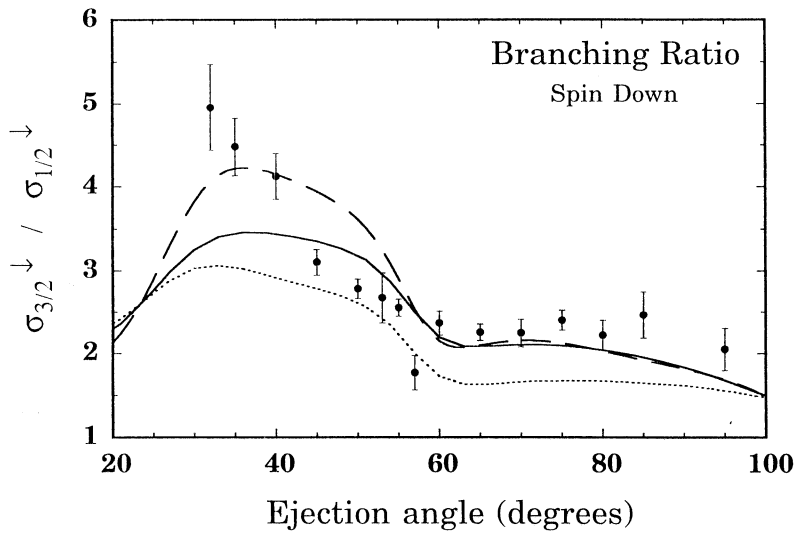

Fig. 11. Spin-resolved branching ratio $\sigma^{\downarrow}_{3/2}/\sigma^{\downarrow}_{1/2}$ for the electron impact ionisation of a ground state Xe target by spin-down incident electrons leading to the Xe^+ $5p^5$ $^2P_{1/2}$ and $^2P_{3/2}$ ion states.

wave functions for the target and ion shows deviation from the ratio of 2 is due to effects attributable to the finite 1·3 eV energy difference between the $^2P_{1/2}$ and $^2P_{3/2}$ transitions incorporated into the calculation to enable comparison with experiment. The calculations using relativistic descriptions of the target wave

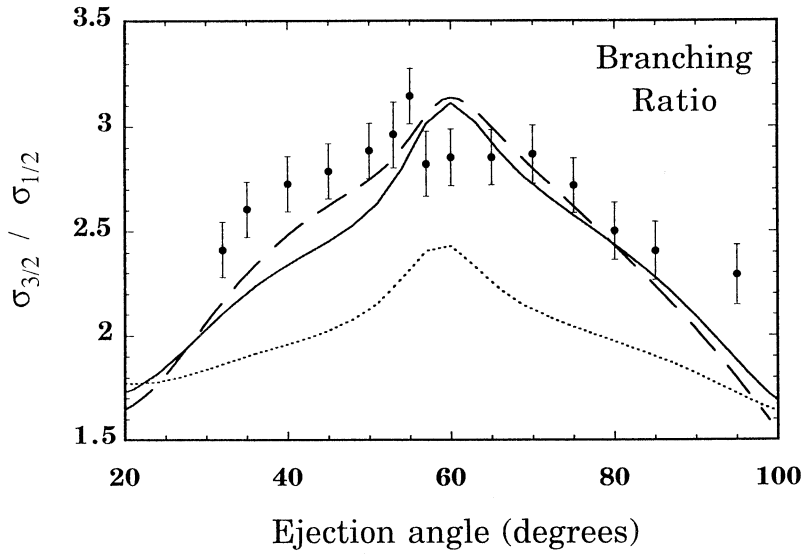

Fig. 12. Spin-averaged branching ratio $\sigma_{3/2}/\sigma_{1/2}$ for the electron impact ionisation of a ground state Xe target leading to the Xe^+ $5p^5$ $^2P_{1/2}$ and $^2P_{3/2}$ ion states. Only the calculations using Dirac–Fock wave functions are able to adequately describe the data. Reaction kinematics and theories are as described above.

function, on the other hand, show much closer agreement with the results of experiment. Thus in contrast to the asymmetry parameter, which provides a sensitive test to the description of the ionisation mechanism, calculation of the branching ratio depends critically on the description of the target.

In the earlier analysis it was noted (equation 5) that, for a 'pure' fine structure effect (i.e. in the limit of negligible spin–orbit interactions of the continuum electrons in the atomic and ionic fields, vanishingly small spin–orbit interaction in the target and residual ion and in the absence of capture), no spin dependence in the ionisation cross section should be observed if the fine structure levels of the final ion state remain unresolved. The large deviations of the unpolarised branching ratio from the value of 2 and large fine structure splitting in the ion, however, show that the assumption of negligible spin–orbit effect in the target is poorly satisfied. Nevertheless, Fig. 13 shows that the residual asymmetry A_{5p} still satisfies the prediction for a 'pure' fine structure effect of zero asymmetry up to 75°, with only a very small non-zero contribution evident above this angle. Note that it follows from equations (5), (12) and (13) that if A_{5p} is identically zero, regardless of whether the spin–orbit interaction or the process of capture plays a small or large role, the following relation holds:

$$A_{1/2}/A_{3/2} = -R\,,$$

which is a modification of the earlier equation (6).

6. Conclusion

The combination of (e, 2e) techniques with polarised electrons and/or polarised targets is a powerful aid to unravelling spin-dependent aspects of the ionisation

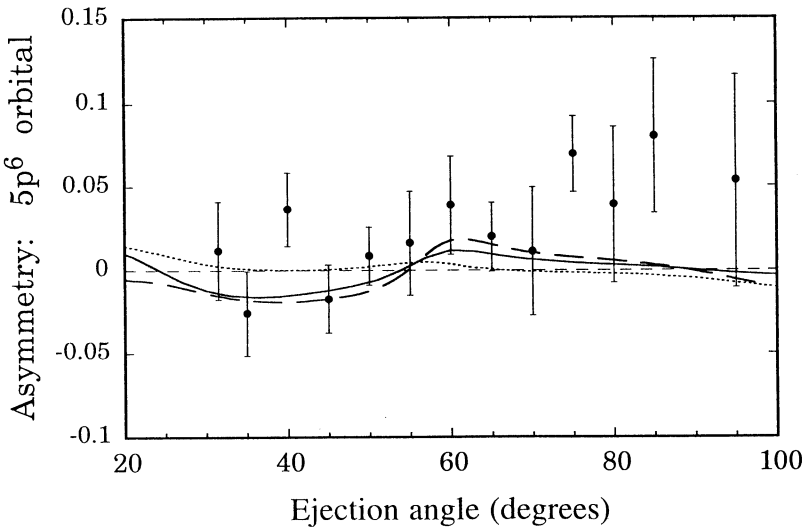

Fig. 13. Residual spin asymmetry A_{5p} for the transition leading to the Xe^+ $5p^5$ ion state, where the $^2P_{1/2}$ and $^2P_{3/2}$ fine structure levels are unresolved. In the limit of negligible spin–orbit interaction and in the absence of capture, this quantity will be zero (see text for details). Reaction kinematics and theories are as above.

process. In our first measurement we have substantiated the existence of an effect analogous to the fine structure effect in excitation. In spite of the fact that xenon is a heavy target, comparison of the measured cross sections with theory suggests the dominant underlying mechanism behind the observed polarisation effects results from the combined effects of collisionally induced orientation of the residual ion formed by the ionisation process and the processes of direct and exchange ionisation. Spin–orbit interaction of the continuum electrons in the atomic and ionic fields and the process of capture appear to play a secondary role under the present kinematics. Comparisons of theory with experiment have shown that whilst our asymmetry measurements provide a stringent test of theories of ionisation, the branching ratio measurements are a stringent test of descriptions of the target wave function. Further measurements and calculations over a broad range of kinematics are presently underway to better disentangle all contributing spin-dependent processes.

Acknowledgments

We kindly thank Professor Don Madison for providing us with his unpublished calculations and for many enlightening discussions.

References

Anderson, N., Gallagher, J. W., and Hertel, I. V. (1988). *Phys. Rep.* **165**, 1.
Baum, G., Blask, W., Freienstein, P., Frost, L., Hesse, S., Raith, W., Rappolt, P., and Streun, M. (1992). *Phys. Rev. Lett.* **69**, 3037.
Brunger, M. J. (1996). *Aust. J. Phys.* **49**, 347.
Dümmler, M., Hanne, G. F., and Kessler, J. (1995). *J. Phys.* B **28**, 2985.
Ehrhardt, H. (1986). *Z. Phys.* D **1**, 3.

Granitza, B., Guo, X., Hurn, J., Shen, Y., and Weigold, E. (1993). Proc. XIV Int. Conf. of the Physics of Electronic and Atomic Collisions', Abstracts of Contributed Papers (Eds T. Andersen *et al.*), p. 201.

Guo, X., Hurn, J. M., Lower, J., Mazevet, S., McCarthy, I. E., Shen, Y., and Weigold, E. (1995). *Phys. Rev. Lett.* (accepted for publication).

Hanne, G. F. (1983). *Phys. Rep.* **95**, 95.

Hanne, G. F. (1991). *In* 'Correlations and Polarisation in Electronic and Atomic Collisions and (e, 2e) Reactions', IOP Conf. Series No. 122 (Eds P. J. O. Teubner and E. Weigold), p. 15 (Institute of Physics: Bristol).

Jones, S., Madison, D. H., and Hanne, G. F. (1994). *Phys. Rev. Lett.* **72**, 2554.

Kessler, J. (1985). 'Polarised Electrons', 2nd edn (Springer: Berlin).

Kessler, J. (1992). Proc. Fifth Physics Summer School on Atomic and Molecular Physics and Quantum Optics (Eds H-A. Bachor *et al.*), p. 65 (World Scientific: Singapore).

Kevan, S. D. (1983). *Rev. Sci. Instrum.* **54**, 1441.

Lower, J., and Weigold, E. (1989). *J. Phys.* E **22**, 421.

McCarthy, I. E., and Weigold, E. (1976). *Phys. Rep.* C **27**, 275.

McCarthy, I. E., and Weigold, E. (1991). *Rep. Prog. Phys.* **54**, 789.

Müller, H., and Kessler, J. (1994). *J. Phys.* B **27**, 5893.

Pierce, D. T., Celotta, R. J., Wang, G.-C., Unertl, W. N., Galejs, A., Kuyatt, C. E., and Mielczarek, S. R. (1980). *Rev. Sci. Instrum.* **51**, 478.

Prinz, H.-Th., Besch, K.-H., and Nakel, W. (1995). *Phys. Rev. Lett.* **74**, 243.

Simon, Th., Laumeyer, N., Hanne, G. F., and Kessler, J. (1993). Seventh Int. Symp. on Polarisation and Correlation in Electronic and Atomic Collisions, Universität Bielefeld (Germany), unpublished.

Manuscript received 10 November, accepted 5 December 1995